World Academy of Science, Engineering and Technology
International Journal of Mechanical and Mechatronics Engineering
Vol:10, No:1, 2016

Autonomous Flight Performance Improvement of Load-Carrying Unmanned Aerial Vehicles by Active Morphing

Tugrul Oktay, Mehmet Konar, Mohamed Abdallah Mohamed, Murat Aydin, Firat Sal, Murat Onay, Mustafa Soylak

***Abstract*—**In this paper, it is aimed to improve autonomous flight performance of a load-carrying (payload: 3 kg and total: 6kg) unmanned aerial vehicle (UAV) through active wing and horizontal tail active morphing and also integrated autopilot system parameters (i.e. P, I, D gains) and UAV parameters (i.e. extension ratios of wing and horizontal tail during flight) design. For this purpose, a load-carrying UAV (i.e. ZANKA-II) is manufactured in Erciyes University, College of Aviation, Model Aircraft Laboratory is benefited. Optimum values of UAV parameters and autopilot parameters are obtained using a stochastic optimization method. Using this approach autonomous flight performance of UAV is substantially improved and also in some adverse weather conditions an opportunity for safe flight is satisfied. Active morphing and integrated design approach gives confidence, high performance and easy-utility request of UAV users.

***Keywords*—**Unmanned aerial vehicles, morphing, autopilots, autonomous performance.

I. Introduction

FOR the previous four and five decades Unmanned Air Vehicles (UAVs) have been extensively applied for military operations and also in commercial requests because of the their numerous advantages with respect to the classical manned vehicles. Some of these advantages are being cheap in manufacturing and operating, flexibility in configuration depending on customer request and they are also not risking the pilot's life on challenging missions. UAVs have also been benefited in aerial agriculture (i.e. crop monitoring and spraying), photography (e.g. film and video), coast guarding (e.g. coastline and see-lane), conservation (e.g. pollution and land monitoring), etc. with civilian purposes. They have also been benefited during military tasks. For instance, they have been applied for navy (e.g. decoying missiles by the emission of artificial signatures and shadowing enemy fleets), army (e.g. reconnaissance and surveillance of enemy activity) and air force (e.g. radar system jamming and destruction and airfield base security). For more UAV applications, [1] can be seen. Many scientific research on UAV design and control have been recently followed (e.g. [2]-[5]).

In classical method, a model of the any physical system will be controlled (e.g. fixed wing UAV, VTOL UAV, helicopter UAV etc.), also named as the "plant", is given a priori to the control system design engineer who has no influence on this model's design. Nonetheless, it is famous fact that the plant design problem and control system design problem are relevant (see [6], [7]). Some small changes in UAV parameters may advance autonomous performance considerably as examined, for example, in [8]-[10]. The classical chronological methodology: first, design the plant, and second design the control system, does not allocate the best overall design (see [6]; [7]). Elegantly, the system required to be controlled and the control system should be simultaneously designed so that a given objective (i.e. cost function) is minimized, while there are rigid constraints on the system and control system parameters. In this paper, this idea is pursued. A load-carrying morphing UAV (i.e. ZANKA-I) manufactured in Erciyes University, College of Aviation and PID based hierarchical autopilot system is simultaneously designed through wing extension and horizontal tail extension parameters and also autopilot P, I, D parameters in order to minimize a cost function consisting of performance parameters, i.e. maximum overshoot, settling time and rise time during trajectory tracking.

Morphing wings for the conventional fixed-wing UAVs have been widely researched recently (see [11], [12]). Morphing parameters can be classified into two general categories: first, wing morphing and second, airfoil morphing. Wing morphing captures variable sweep, dihedral, twist, span. However, airfoil morphing captures variable airfoil thickness, chord length, and camber. It is also possible that combination of wing morphing and airfoil morphing can be considered together. In this paper, wing morphing (i.e. span morphing or extension) is considered and a load-carrying (3 kg payload) UAV (total of 6 kg) is equipped with span morphing wing and horizontal tail. Their design is examined simultaneously with autopilot system for best autonomous performance.

Autopilots are devises for guiding UAVs for the period of flight without any assistance of human workers. Autopilots are onboard intelligent systems and consist of state sensors and controllers. State sensors constantly measure various parameters of UAV using multiple sensors (e.g. GPS, accelerometer, magnetometer, gyros, pitot-tube). Control systems use these measurements and calculate the error between current and required states. The control signals depend on the error signal and this signal is produced to actuate the various control surfaces of the aircraft. Due to reality that aircraft dynamics is exceedingly nonlinear, many

T. Oktay is with the Erciyes University, Kayseri, 38039 Turkish Republic (corresponding author to provide phone: +90-533-5186324; e-mail: tugruloktay52@ gmail.com).

M. Konar, M. Abdallah Mohamed, M. Aydin, F. Sal, M. Onay, and M. Soylak are with the Erciyes University, Kayseri, 38039 Turkish Republic.

intelligent control methods, e.g., PID control, neural network, fuzzy logic, sliding mode control, etc. have been used for autopilots in order to talent a smooth appropriate trajectory navigation (see [13] for more discussion). In this conference article, an autopilot system having PID based hierarchical control structure is benefited. Recently, PID based controllers have been used by different researches effectively (e.g. see [14], [15]).

This is the *one of uncommon articles* simultaneously designing a load-carrying morphing UAV and autopilot system for autonomous performance maximization. Moreover, for this drive a stochastic optimization method (i.e. SPSA, simultaneous perturbation stochastic approximation) is *first time* benefited and using it, optimal results are found safely and fast. In addition, simultaneous design idea during morphing case progresses autonomous flight performance noticeably, therefore less overshoot, less settling time and less rise time are obtained during trajectory tracking.

II. UAV Model

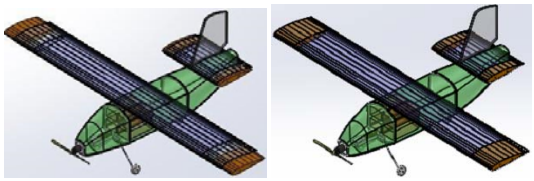

(a) (b)

Fig. 1 ZANKA-II (a) non-morphed (b) morphed

Longitudinal and lateral linearized state-space models of a fixed-wing aircraft UAV are given in (1) and (2), respectively [16]:

$$\underbrace{\begin{bmatrix}\Delta\dot{u}\\ \Delta\dot{w}\\ \Delta\dot{q}\\ \Delta\dot{\theta}\\ \Delta\dot{h}\end{bmatrix}}_{\dot{x}_l} = \underbrace{\begin{bmatrix} X_u & X_w & 0 & -g & 0\\ Z_u & Z_w & u_0 & 0 & 0\\ M_u+M_{\dot{w}}Z_w & M_w+M_{\dot{w}}Z_w & M_q+M_{\dot{w}}u_0 & 0 & 0\\ 0 & 0 & 1 & 0 & 0\\ -\sin(\theta_0) & \cos(\theta_0) & 0 & -u_0\cos(\theta_0) & 0\end{bmatrix}}_{A_l} \underbrace{\begin{bmatrix}\Delta u\\ \Delta w\\ \Delta q\\ \Delta\theta\\ \Delta h\end{bmatrix}}_{x_l} + \underbrace{\begin{bmatrix} X_{\delta_T} & X_{\delta_e}\\ Z_{\delta_T} & Z_{\delta_e}\\ M_{\delta_T}+M_{\dot{w}}Z_{\delta_T} & M_{\delta_e}+M_{\dot{w}}Z_{\delta_e}\\ 0 & 0\\ 0 & 0\end{bmatrix}}_{B_l} \underbrace{\begin{bmatrix}\Delta\delta_T\\ \Delta\delta_e\end{bmatrix}}_{u_l} \tag{1}$$

$$\underbrace{\begin{bmatrix}\Delta\dot{\beta}\\ \Delta\dot{p}\\ \Delta\dot{r}\\ \Delta\dot{\phi}\\ \Delta\dot{\psi}\end{bmatrix}}_{\dot{x}_{la}} = \underbrace{\begin{bmatrix} \frac{Y_\beta}{u_0} & \frac{Y_p}{u_0} & -(1-\frac{Y_r}{u_0}) & -\frac{g}{u_0}\cos(\theta_0) & 0\\ L^*_\beta+\frac{I_{xz}}{I_{xx}}N^*_\beta & L^*_p+\frac{I_{xz}}{I_{xx}}N^*_p & L^*_r+\frac{I_{xz}}{I_{xx}}N^*_r & 0 & 0\\ N^*_v+\frac{I_{xz}}{I_{zz}}L^*_v & N^*_p+\frac{I_{xz}}{I_{zz}}L^*_p & N^*_r+\frac{I_{xz}}{I_{zz}}L^*_r & 0 & 0\\ 0 & 1 & 0 & 0 & 0\\ 0 & 0 & \sec(\theta_0) & 0 & 0\end{bmatrix}}_{A_{la}} \underbrace{\begin{bmatrix}\Delta\beta\\ \Delta p\\ \Delta r\\ \Delta\phi\\ \Delta\psi\end{bmatrix}}_{x_{la}} + \underbrace{\begin{bmatrix} 0 & \frac{Y_{\delta_r}}{u_0}\\ L^*_{\delta_a}+\frac{I_{xz}}{I_{xx}}N^*_{\delta_a} & L^*_{\delta_r}+\frac{I_{xz}}{I_x}N^*_{\delta_r}\\ N^*_{\delta_a}+\frac{I_{xz}}{I_{zz}}L^*_{\delta_a} & N^*_{\delta_r}+\frac{I_{xz}}{I_{zz}}L^*_{\delta_r}\\ 0 & 0\\ 0 & 0\end{bmatrix}}_{B_{la}} \underbrace{\begin{bmatrix}\Delta\delta_a\\ \Delta\delta_r\end{bmatrix}}_{u_{la}} \tag{2}$$

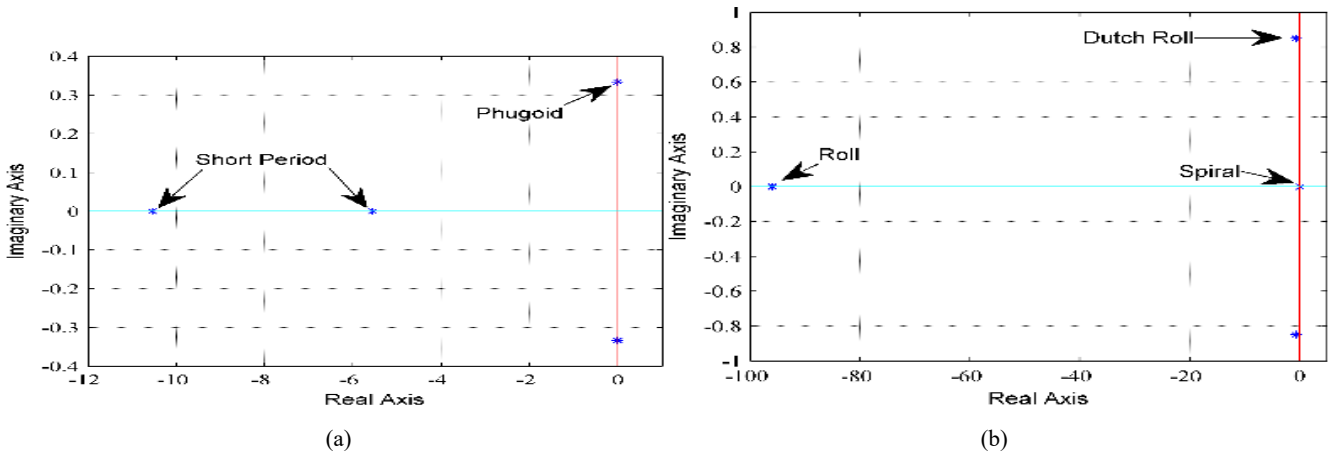

(a) (b)

Fig. 2 (a) Longitudinal, (b) Lateral Flight Dynamics Modes

The longitudinal and lateral flight dynamics modes of UAV (i.e. ZANKA-II) are given in Fig. 2. From these figures, it can be clearly seen that qualitative and quantitative behaviors of flight dynamics modes are similar with the ones given in [17]-[21]. When gust disturbance exists, the parametrical state-space models are:

$$\underbrace{\begin{bmatrix}\Delta\dot{u}\\ \Delta\dot{w}\\ \Delta\dot{q}\\ \Delta\dot{\theta}\end{bmatrix}}_{\dot{x}_l} = \underbrace{\begin{bmatrix} X_u & X_w & 0 & -g\\ Z_u & Z_w & u_0 & 0\\ M_u+M_wZ_w & M_w+M_wZ_w & M_q+M_wu_0 & 0\\ 0 & 0 & 1 & 0\end{bmatrix}}_{A_l}\underbrace{\begin{bmatrix}\Delta u\\ \Delta w\\ \Delta q\\ \Delta\theta\end{bmatrix}}_{x_l} + \underbrace{\begin{bmatrix} X_{\delta_T} & X_{\delta_e}\\ Z_{\delta_T} & Z_{\delta_e}\\ M_{\delta_T}+M_wZ_{\delta_T} & M_{\delta_e}+M_wZ_{\delta_e}\\ 0 & 0\end{bmatrix}}_{B_l}\underbrace{\begin{bmatrix}\Delta\delta_T\\ \Delta\delta_e\end{bmatrix}}_{u_l} + \underbrace{\begin{bmatrix} -X_u & -X_w & 0\\ -Z_u & -Z_w & 0\\ -M_u & -M_w & -M_q\\ 0 & 0 & 0\end{bmatrix}}_{B_{l_{gust}}}\underbrace{\begin{bmatrix}u_g\\ w_g\\ q_g\end{bmatrix}}_{u_{l_{gust}}} \tag{3}$$

$$\underbrace{\begin{bmatrix}\Delta\dot{\beta}\\ \Delta\dot{p}\\ \Delta\dot{r}\\ \Delta\dot{\phi}\end{bmatrix}}_{\dot{x}_{la}} = \underbrace{\begin{bmatrix} \frac{Y_\beta}{u_0} & \frac{Y_p}{u_0} & -(1-\frac{Y_r}{u_0}) & -\frac{g}{u_0}\cos(\theta_0)\\ L^*_\beta+\frac{I_{xz}}{I_{xx}}N^*_\beta & L^*_p+\frac{I_{xz}}{I_{xx}}N^*_p & L^*_r+\frac{I_{xz}}{I_{xx}}N^*_r & 0\\ N^*_v+\frac{I_{xz}}{I_{zz}}L^*_v & N^*_p+\frac{I_{xz}}{I_{zz}}L^*_p & N^*_r+\frac{I_{xz}}{I_{zz}}L^*_r & 0\\ 0 & 1 & 0 & 0\end{bmatrix}}_{A_{la}}\underbrace{\begin{bmatrix}\Delta\beta\\ \Delta p\\ \Delta r\\ \Delta\phi\end{bmatrix}}_{x_{la}} + \underbrace{\begin{bmatrix} 0 & \frac{Y_{\delta_r}}{u_0}\\ L^*_{\delta_a}+\frac{I_{xz}}{I_{xx}}N^*_{\delta_a} & L^*_{\delta_r}+\frac{I_{xz}}{I_x}N^*_{\delta_r}\\ N^*_{\delta_a}+\frac{I_{xz}}{I_{zz}}L^*_{\delta_a} & N^*_{\delta_r}+\frac{I_{xz}}{I_{zz}}L^*_{\delta_r}\\ 0 & 0\end{bmatrix}}_{B_{la}}\underbrace{\begin{bmatrix}\Delta\delta_a\\ \Delta\delta_r\end{bmatrix}}_{u_{la}} + \underbrace{\begin{bmatrix} -\frac{Y_\beta}{u_0} & 0 & 0\\ -L^*_\beta\frac{I_{xz}}{I_{xx}}N^*_\beta & -L^*_p\frac{I_{xz}}{I_{xx}}N^*_p & -L^*_r\frac{I_{xz}}{I_{xx}}N^*_r\\ -N^*_v\frac{I_{xz}}{I_{zz}}L^*_v & -N^*_p\frac{I_{xz}}{I_{zz}}L^*_p & -N^*_r\frac{I_{xz}}{I_{zz}}L^*_r\\ 0 & 0 & 0\end{bmatrix}}_{B_{la_{gust}}}\underbrace{\begin{bmatrix}v_g/u_0\\ p_g\\ r_g\end{bmatrix}}_{u_{la_{gust}}} \tag{4}$$

For this paper, Von-Karman Turbulence modeling approach is used [22].

III. Autopilot System

For our both theoretical and practical (with real-time flight tests) studies, traditional PID based hierarchical autopilot system is chosen [13], [23]. It uses three layers PID controller to accomplish waypoint navigation (see Fig. 3). In Fig. 4 more detailed version of PID-based hierarchical autopilot system is given. In Fig. 5, an Ardupilot equipped ZANKA-II is given.

IV. Mechanism of Morphing Wing Tip

Aircraft or air vehicles wings are a compromise that allows the aircraft to fly at a range of flight conditions, but the performance at each condition is sub-optimal. Mechanisms such as deployable flaps, wing tips which provide the ability of a wing surface to change its geometry during flight has interested researchers and designers over the years as this reduces the design compromises required. Placing mechanical elements on the wing tips and according to specified values given by remote control extension of wing tips is provided and thus, wing area increases. Main Components of the system;

- Reductive Micro Motor,
- Two equal number of gear teeth,
- M3 worm gear,
- Bidirectional mini Brushing ESC.

The system is composed of the simple association of the elements listed. As shown in Fig. 6, micro motor is a DC motor which operates between range 6-9 V range and produces a torque of 1.8 Kg. A gear motor is mounted to the shaft of this motor. This gear works together with a second gear mounted on a bearing (Figs. 7 and 8).

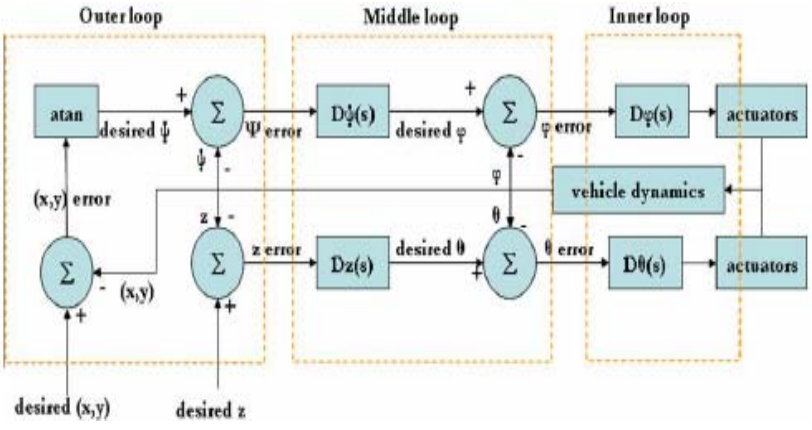

Fig. 3 Hierarchical Autopilot System (taken from [13])

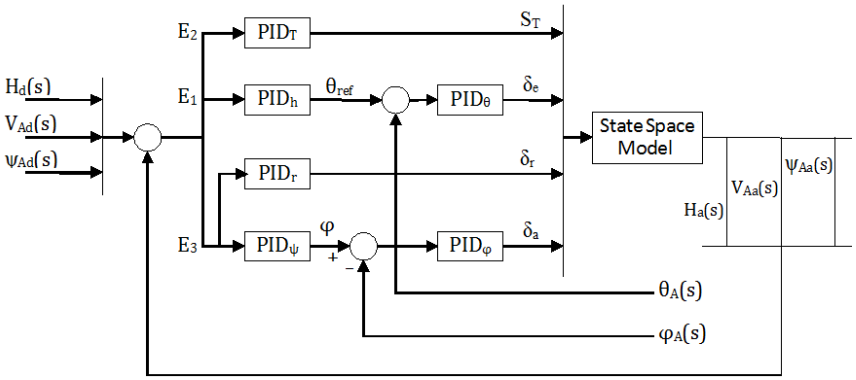

Fig. 4 PID Based Autopilot Structure

Fig. 5 Autopilot Equipment of ZANKA-II

Fig. 6 DC Motor and Gear Motor Mounted to Shaft

Fig. 7 Placement of the Servo Motor in the Wing

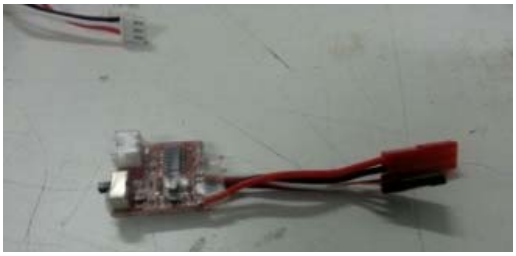

Fig. 8 Electronic Speed Controller

Fig. 9 Montage of the Expanding Parts of the Wing

Fig. 10 3D View of the Over-Expanding Part of the Wing

Fig. 11 Morphing Wing Tip Assembly

Interior of the gear mounted on bearing has M3 tooth in opened state. Signal sent to ESC through a bistable switch defined on the remote control gives the engine right or left turn. ESC is a brushed and bidirectional circuit and according to the directly incoming signal through remote control switch works in two ways (Fig. 9). Motor and therefore mechanical

systems which move according to the direction of rotation of gears lead worm screw in-or-outward (Fig. 10). This movement results by moving wing tips parts, produced by outer mold method, over main section so thus to provide the variation of the wing area.

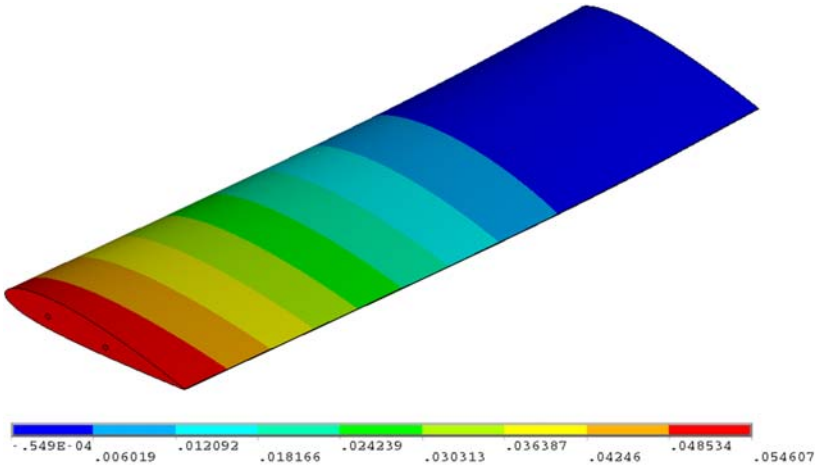

(i)

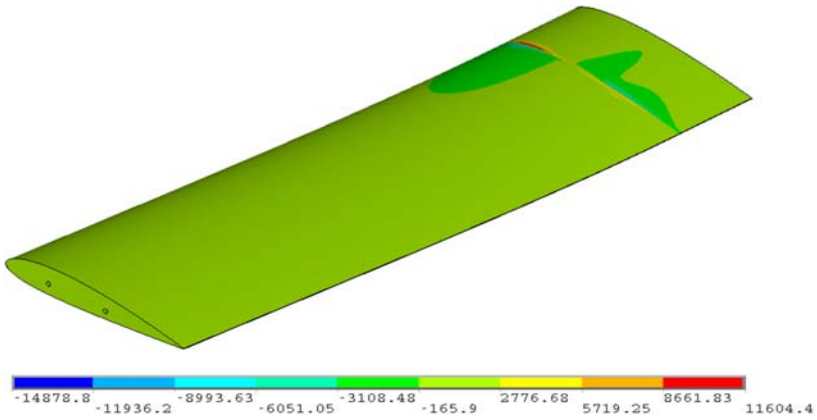

(ii)

(a) Before Morphing (i) meters (ii) Pascal

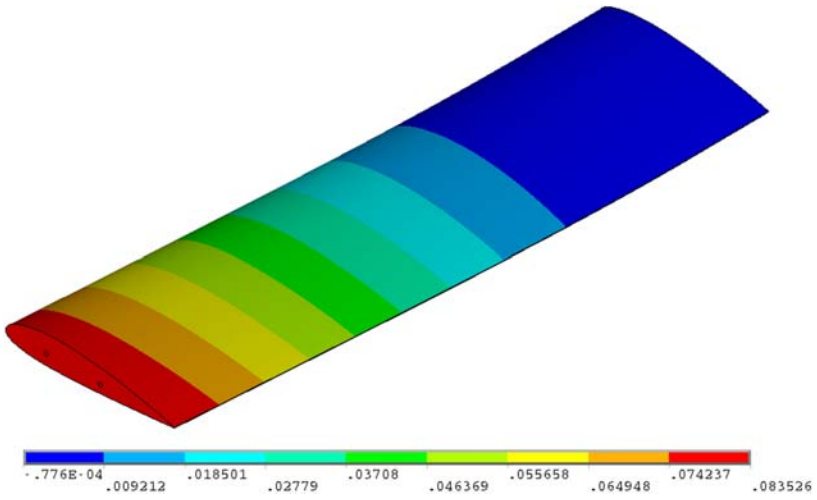

(i)

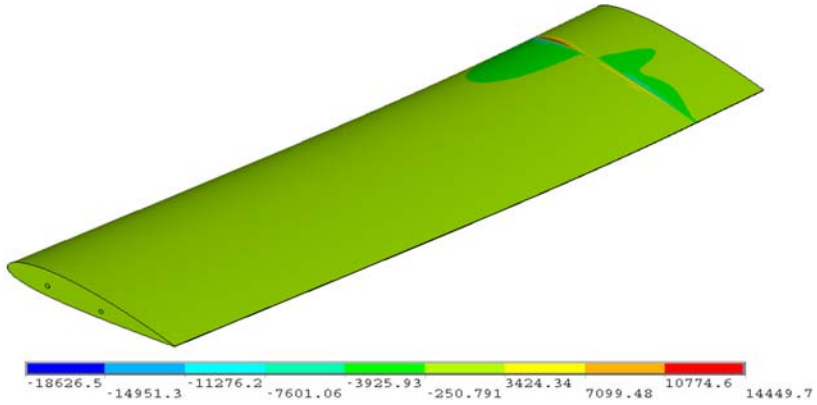

(ii)

(b) After Morphing (i) meters (ii) Pascal

Fig. 12 (a) Deformation, (b) Shear Stresses for Morphing Wing

In order to make the movement healthier and synchronized, expansion shell is supported also with Carbone shafts. Thus, the same mechanical systems, without compression and equidistantly from both wing tips, will perform changes (see Fig. 11). As a result, this mechanical metamorphosis systems; either on main wing or on the rising; as shown in Fig. 8, need integrity without visual difference and obstacles in external parts and the mechanical metamorphosis systems work.

For 60 km/h straight level flight condition, using ANSYS software results of deformations and shear stresses of morphing wing are given in Fig. 12 when two carbon beams exist inside of the wing. From this figure it can be easily ascertained that for this flight condition our 3 kg payload carrying 6 kg UAV (i.e. ZANKA-II) do not structurally fail during flight.

V. Structural Pre Test

Fig. 14 shows the deflection values for the along the wings of UAV. Deflection increases along the wing tip so reaches peak value in the remotest point of wings. Fig. 15 shows von Misses stress values for the along the wings of UAV. The von Misses stresses vary throughout the wing length by reason of decreasing bending stiffness of wing consequentially the largest von Misses stresses were obtained at the part of the wing root. For the best location of the carbon tubes, the maximum stress value is under the yield stress of foam and carbon tubes.

Stress values of the wing, manufactured from an extruded rigid polystyrene foam sheets (STYROFOAM IBF) and containing carbon tube on the locations providing maximum strength, are under yield stress and therefore material strength is safe.

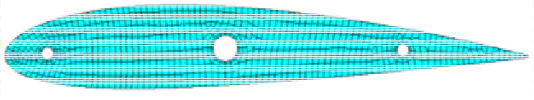

Fig. 13 Finite Element Model of the Wing

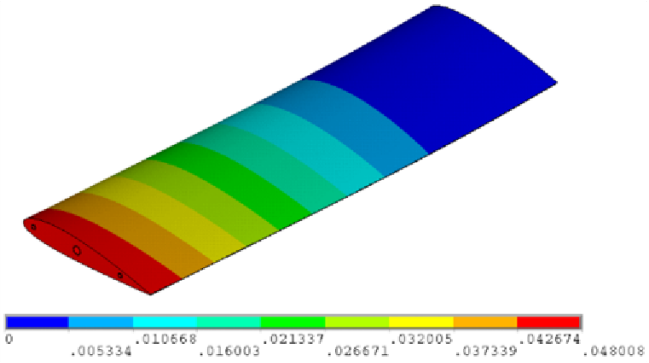

Fig. 14 Deflection Distribution along the Wing (meter)

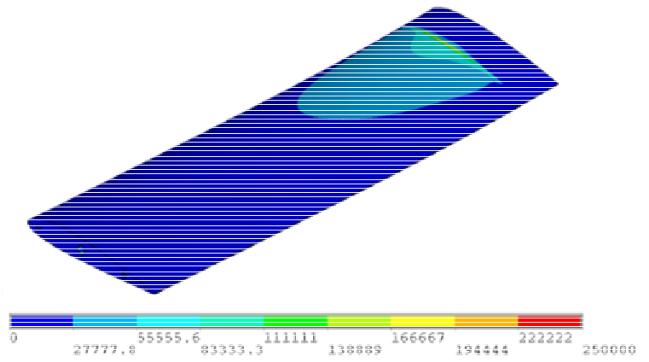

Fig. 15 Von Mises Stress Distribution along the Wings (Pascal)

Deformation along chord line of the wing tip and wing span are given respectively in Figs. 16 (quarter chord) and 17. While examining graphics a twist of 0.54 degree along chord line of wing direction and an inclination of 4.5 degree along the wing occur.

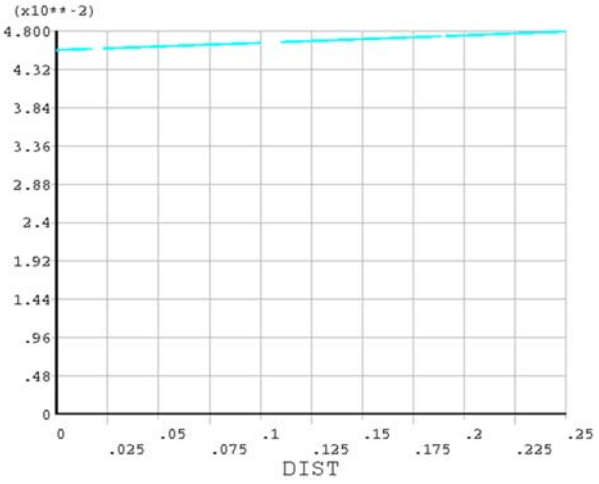

Fig. 16 Deformation along Chord Line of the Wing Tip

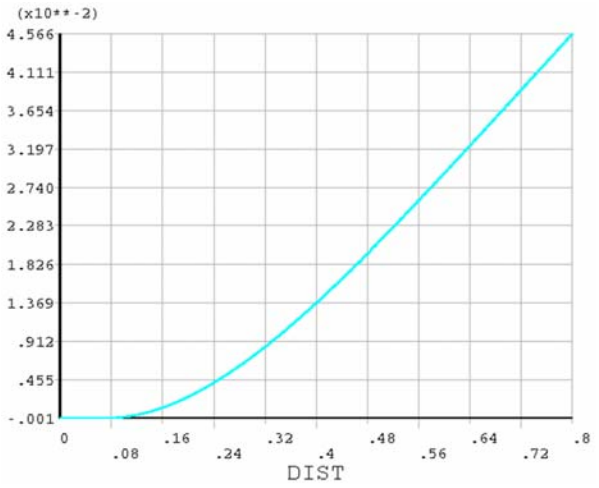

Fig. 17 Deformation along Wing Span

VI. Problem Formulation and Optimization Technique (i.e. SPSA)

In most general form PID based hierarchical autopilot system permits height, yaw angle, and velocity tracking tracking. These systems have 6 P-I-D controllers in 3 layers (outer, middle, inner). These PIDs have upper and lower bounds and satisfy trajectory tracking. If any interested autopilot user requests to benefit from all of them, it is required to tune 18 parameters (i.e. 6 P parameters, 6 I parameters and 6 D parameters). Nonetheless, in this conference article for simultaneous morphing UAV and control system (i.e. autopilot) design idea there are two additional structural parameters (optimum extension ratios of wing and horizontal tail). A cost function consisting of settling time, rise time and overshoot is respectable choice for high-performance trajectory tracking (see (5)).

$$\boldsymbol{J} = T_{st} + T_{rt} + \%OS \tag{5}$$

The simultaneous optimization problem can be defined as: $min\{\boldsymbol{J}\}$ where

$$\boldsymbol{J} = f\left(x\_w\_morph, x\_ht\_morph, K_{P_1}, K_{I_1}, K_{D_1}, K_{P_2}, K_{I_2}, K_{D_2}, \ldots\ldots\ldots\ldots, K_{P_6}, K_{I_6}, K_{D_6}\right) \tag{6}$$

and it is function of 20 terms (2 UAV morphing parameters and 18 autopilot system design parameters). Terms of cost function is calculated in this conference article as:

If $T_{st} \geq T_{st_u}$, T_{st} is non-defined else

$T_{st} < T_{st_u}$, T_{st} is its value (7a)

If $T_{rt} \geq T_{rt_u}$, T_{rt} is non-defined else,

$T_{rt} < T_{rt_u}$, T_{rt} is its value (7b)

If $\%OS \geq \%OS_u$, $\%OS$ is non-defined else $\%OS < \%OS_u$, $\%OS$ is its value (7c)

A. Simultaneous Perturbation Stochastic Approximation (SPSA)

Since there is complex dependency between $\boldsymbol{J}$ (see (6)) and the constraints on the optimization variables (18 P-I-D gains and 2 UAV morphing parameters, total of 20 parameters), computation of cost function derivatives with respect to these parameters is analytically impossible. This supports the demand of certain stochastic optimization techniques. In order to solve this problem we select a stochastic optimization method called as SPSA, which was successfully used in similar complex constrained optimization problems previously (see [24-[26]). SPSA has many advantages w.r.t. the other existing method in the literature. First, SPSA is inexpensive because it uses only two evaluations of the objective to estimate the gradient (see [27]). Moreover, it is also successful in solving constrained optimization problems (see [24]-[26]). Its short description is given next.

Let Ψ denote the vector of optimization variables. For the classical SPSA, if $\Psi_{[k]}$ is the estimate of Ψ at k-th iteration, then $\Psi_{[k+1]} = \Psi_{[k]} - \Psi_k g_{[k]}$, where

$$g_{[k]} = \left[\frac{\Gamma_+ - \Gamma_-}{2d_k\Delta_{[k]1}} \ldots\ldots \frac{\Gamma_+ - \Gamma_-}{2d_k\Delta_{[k]p}}\right]^T \tag{8}$$

a_k and d_k are gain sequences, $g_{[k]}$ is the estimate of the objective's gradient at $\Psi_{[k]}$, $\Delta_{[k]} \in R^p$ is a vector of p mutually independent mean-zero random variables $\{\Delta_{[k]1} \ldots\ldots \Delta_{[k]p}\}$ fulfilling certain requirements (see [27], [28]), Γ_+ and Γ_- are estimates of the objective evaluated at $\Psi_{[k]} + d_k\Delta_{[k]}$ and $\Psi_{[k]} - d_k\Delta_{[k]}$, respectively. The adaptation is through using gain sequences a_k and d_k, which is required to change according to

$$a_k = \min\left\{a/(S+k)^{\lambda}, 0.95\min_i\left\{\min(\mu_{l_i}), \min(\mu_{u_i})\right\}\right\} \quad (9a)$$

$$d_k = \min\left\{d/k^{\Theta}, 0.95\min_i\left\{\min\left\{\eta_{l_i}\right\}, \min\left\{\eta_{u_i}\right\}\right\}\right\} \quad (9b)$$

where η_l and η_u are vectors whose components are $(\Psi_{[k]i} - \Psi_{min_i})/\Delta_{[k]i}$ for each positive $\Delta_{[k]i}$ and $(\Psi_{max_i} - \Psi_{[k]i})/\Delta_{[k]i}$ for each negative $\Delta_{[k]i}$, respectively. In similar way, μ_l and μ_u are vectors whose components are $(\Psi_{[k]i} - \Psi_{min_i})/g_{[k]i}$ for each positive $g_{[k]i}$ and $(\Psi_{[k]i} - \Psi_{max_i})/g_{[k]i}$ for each negative $g_{[k]i}$, respectively and d, a, λ, Θ, S are other SPSA parameters.

B. Algorithm of SPSA For Simultaneous Morphing UAV and Autopilot System Design

Step 1: Set k=1 and choose initial values for the optimization parameters, $\Psi = \Psi_{[k]}$, and a specific flight condition (e.g. straight level flight at speed $V_A = 60$ km/h).

Step 2: Compute A_p and B_p, design the corresponding autopilot system and obtain the current value of the objective, Γ_k given by (6) (note that $\Gamma_k = J_k$ for our autopilot system).

Step 3: Perturb $\Psi_{[k]}$ to $\Psi_{[k]} + d_k\Delta_{[k]}$ and $\Psi_{[k]} - d_k\Delta_{[k]}$ and solve the corresponding autopilot system in order to obtain Γ_+ and Γ_-, respectively. Then compute the approximate gradient, $g_{[k]}$, using (8) with d_k given by (9b).

Step 4: If $\left\|a_k g_{[k]}\right\| < \delta\Psi$, where a_k is given by (9a) and $\delta\Psi$ is the minimum allowed variation of Ψ, or k+1 is greater than the maximum number of iterations allowed, exit, else calculate the next estimate of Ψ, $\Psi_{[k+1]}$, using $\Psi_{[k+1]} = \Psi_{[k]} - a_k g_{[k]}$, set k=k+1 and return to Step 2.

VII. Simultaneous Morphing UAV and Autopilot System Design Results

Morphing load-carrying UAV (i.e. ZANKA-II) and autopilot system (for pitch attitude tracking) are simultaneously designed in order to minimize cost function (see (5)) using SPSA. For this conference article the ZANKA-II UAV was tracking a 5 degrees of pitch angle and there were a PID controller parameters and two moprhing parameters (i.e. wing and horizontal tail) during this optimization problem. SPSA parameters applied were: S=5, a=100, λ=0.602, d=20, Θ=0.101. After 10 iterations optimum parameters found were: $x\_w\_morph = 0.2665$, $x\_ht\_morph = 0.2875$, $K_{P_\theta} = 73.3561$, $K_{I_\theta} = 2.5070$, $K_{D_\theta} = 74.9973$. In Fig. 7, response of ZANKA-II for desired pitch angle, cost minimization during using SPSA, and relative energy save at each iteration are given. The relative energy save $\%J$ is: $\%J = 100(J_0 - J_f)/J_0$ where J_0 and J_f are costs of performance for initial and final situations, respectively.

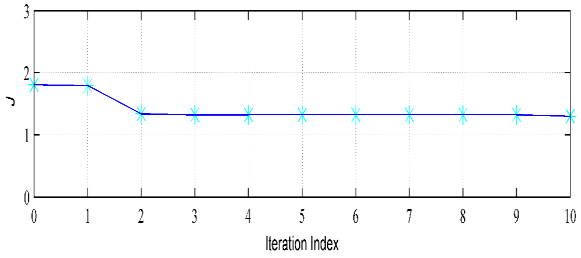

(a)

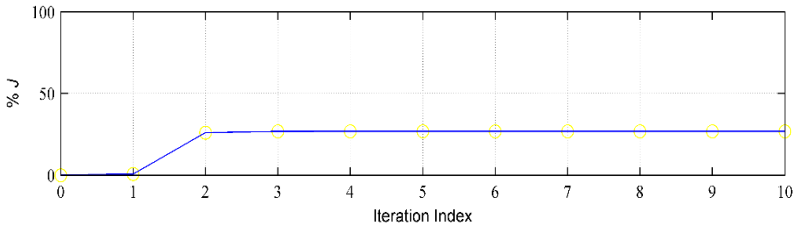

(b)

Fig. 18 (a) SPSA Application, (b) Relative Energy Save

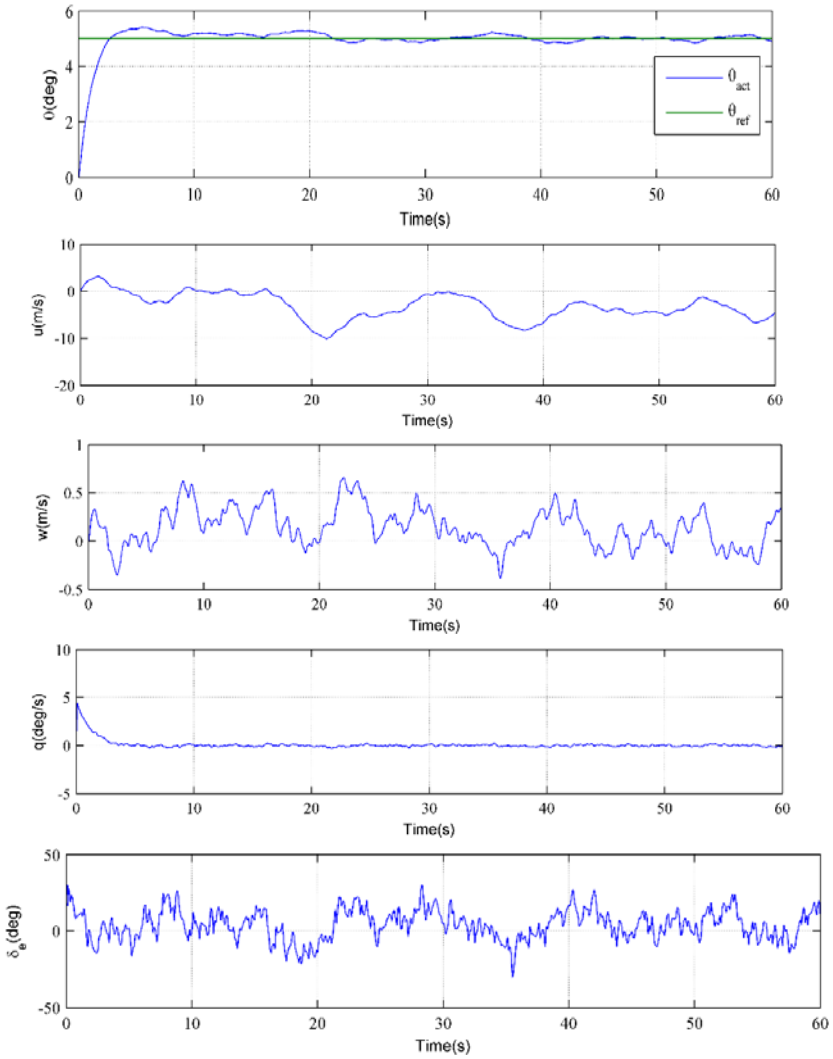

Fig. 19 Simulation Results

From Figs. 18 and 19 it can be said that autopilot system is very successful during tracking reference trajectory. Moreover, SPSA is very fast and effective during energy minimization. Finally, substantial energy (around %27) is saved using simultaneous morphing UAV and autopilot system design.

VIII. Simulation Results

Achievement of applied autopilot system when there is turbulence on the system (i.e. pure turbulence) is also investigated. In Fig. 19 the closed loop system responses when there is pure turbulence on the system are given. From this figure, it can be ascertained that when there is also turbulence on the system, the autopilot system is able to track reference trajectory effectively. Furthermore, other states do not experience catastrophic behavior (fast and large oscillations) during this pitch trajectory tracking. Final, while there is constraint on control surface (+-30 degrees for elevator), it is also achievable for desired trajectory tracking.

IX. Conclusions

Simultaneous morphing load carrying (i.e. 3 kg payload) unmanned aerial vehicle (UAV) (total of 6 kg) and autopilot system design is investigated in order to progress autonomous flight performance of UAVs. Dynamic modeling of a fixed-wing aircraft is shortly presented. Obtained models are validated using existing data in the literature. A PID based hierarchical autopilot system is applied for this conference study. A stochastic optimization method namely simultaneous perturbation and stochastic approximation (i.e. SPSA) is applied for autonomous performance maximation. Important improvement in flight performance (around %27) is obtained using simultaneous morphing UAV and autopilot system design idea. This satisfied the general requirements of less overshoot, less settling and less rise time for UAVs. Closed-loop responses when there is pure turbulence during flight is also examined and acceptable results (meaning that small rise and settling time and small overshoot) are found. This conference article study gives UAV users confidence, high performance, and easy utility.

ACKNOWLEDGMENT

This work was supported by Research Fund of The Scientific and Technological Research Council of Turkey (**TÜBİTAK**) under Project Number: 214M282.

The authors would like to thank Mr. Orhan Kizilkaya and Mr. Hasan Murat Sert for their technical supports during this study and also would like to thank Prof. Dr. Mustafa Kemal Apalak for serving opportunities of Erciyes University, Faculty of Aeronautics and Astronautics.

REFERENCES

[1] Austin, R. 2010. Unmanned aircraft systems. Wiley.
[2] Dink, Y., Liu, Y. C., and Hsiao, F. B. The application of extended Kalman filtering to autonomous formation flight of small UAV system. *Aircraft Engineering and Aerospace Technology*. 1(2), 154-186.
[3] Drak, A., Hejase, M., ElShorbagy, M., Wahyudie, A., & Noura, H. 2014. Autonomous Formation Flight Algorithm and Platform for Quadrotor UAVs. *International Journal of Robotics and Mechatronics*. 1(4), 124-132.
[4] Luca De Filippis, Giorgio Guglieri, Fulvia B. Quagliotti. 2014. A novel approach for trajectory tracking of UAVs. *Aircraft Engineering and Aerospace Technology: An International Journal*. 86 (3), 198 – 206.
[5] Hadi, G., Varianto, R., Trilaksono, B., and Budiyono, A. 2014. Autonomous UAV System Development for Payload Dropping Mission. *Journal of Instrumentation, Automation, and Systems*. 1(2), 72-77.
[6] Grigoriadis, K. M., Carpenter, M. J. Zhu, G., and Skelton, R. E. 1993. Optimal Redesign of Linear Systems. Paper presented at Proceedings of the American Control Conference, San Francisco, CA.
[7] Grigoriadis, K. M., Zhu, G., and Skelton, R. E. 1996. Optimal Redesign of Linear Systems. *Journal of Dynamic Systems, Measurement, and Control*. 118 (3), 598–605.
[8] Krog, L., Tucker, A., Kemp, M., and Boyd, R. 2004. Topology Optimization of Aircraft Wing Box Ribs. Paper presented at 10th AIAA/ISSMO Multidisciplinary Analysis and Optimization Conference. Albany, New York, USA.
[9] Park, K., Han, J. W., Lim, H. J., Kim, B. S. and Lee, J. 2008. Optimal Design of Airfoil with High Aspect Ratio in Unmanned Aerial Vehicles. *World Academy of Science, Engineering and Technology*, 2 (4), 171-177.
[10] Qun, W. and Hong-quang, J. 2011. Optimal design of UAV's pod shape. Paper presented at International Symposium on Photoelectronic Detection and Imaging: Advances in Infrared Imaging and Applications Beijing, China.
[11] Moosavian, A., Xi, F., and Hashemi, S. M. 2013. Design and Motion Control of Fully Variable Morphing Wings. *Journal of Aircraft*. 50(4), 1189-1201.
[12] Yue, T. and Wang, L. 2013. Longitudinal Linear Parameter Varying Modeling and Simulation of Morphing Aircraft. *Journal of Aircraft*. 50(6), 1673-1681.
[13] Chao, H., Cao, Y., and Chen, Y. Q. 2007. Autopilots for Small Fixed-Wing Unmanned Aerial Vehicles: A Survey. Paper presented at IEEE International Conference on Mechatronics and Automation, Harbin, China.
[14] Jung, D., Ratti, J., Tsiotras, P. 2009. Real-time implementation and validation of a new hierarchical path planning scheme of UAVs via hardware-in-the-loop simulation. *Journal of Intelligent and Robotic Systems*, 54 (1-3), 163-281.
[15] Sartori, D. 2014. Design, implementation, and testing of advanced control laws for fixed-wing UAVs. PhD dissertation, Politecnico di Torino, Torino, Italy.
[16] Nelson, R. C. 2007. Flight Stability and Automatic Control. 2nd ed., McGraw-Hill, New York, chapters 2-6.
[17] Zagi-The original R/C EPP foam wing homepage (2015), http//:www.zagi.com.
[18] Vural, S. Y. and Hajiyev, C. 2008. Autopilot system design for a small unmanned aerial vehicle. MS thesis, Istanbul Technical University, Istanbul, Turkey.
[19] Vural, S. Y. and Hajiyev, C. 2013. LQR controller with Kalman estimator applied to UAV longitudinal dynamics. *Scientific Research Journal*. 4, 36-41.
[20] Cardenas, E. M., Boschetti, P. J., and Celi, M. R. 2012. Design of control systems to hold altitude and heading in severe atmospheric disturbances for an unmanned airplane. Paper presented at 50th AIAA Aerospace Sciences Meeting including the New Horizons Forum and Aerospace Exposition, Nashville, Tennessee.
[21] Jeni, S. D. and Budiyono, A. 2006. Automatic Flight Control System", Lecture notes for Malaysian Institute of Aviation Technology.
[22] U.S. Military Handbook MIL-HDBK-1797, 1997.
[23] Jang, J. S., Liccardo, D. 2006. Automation of small UAVs using a low cost mems sensor and embedded computing platform.
[24] Sultan, C. 2010. Proportional damping approximation using the energy gain and simultaneous perturbation stochastic approximation. Mechanical Systems and Signal Processing. 24, 2210-2224.
[25] Oktay, T. 2012. Constrained control of complex helicopter models. PhD Dissertation, Virginia Tech.
[26] Oktay, T. and Sultan, C. (2013), "Simultaneous helicopter and control-system design," *Journal of Aircraft*, Vol. 50, No. 3, pp. 32-47.
[27] Sadegh, P. and Spall, J. C. (1998), "Optimal random perturbations for multivariable stochastic approximation using a simultaneous perturbation gradient approximation", IEEE Transactions on Automatic Control, 43(10), pp. 1480-1484.
[28] He, Y. and Fu, M. C. (2003), "Convergence of simultaneous perturbation stochastic approximation for non-differentiable optimization", IEEE Transactions on Aerospace and Electronic Systems, 48 (8), 1459-1463.